A High-Accuracy Multidomain Legendre Pseudospectral Frequency-Domain Method With Penalty Scheme for Solving Scattering and Coupling Problems of Nano-Cylinders

Chih-Yu Wang, Shih-Yung Chung, Chun-Hao Teng, Juen-Kai Wang, Chung-Ping Chen, *Member, IEEE*, and Hung-chun Chang, *Senior Member, IEEE, Fellow, OSA*

***Abstract*—A new multidomain pseudospectral frequency-domain (PSFD) method based on the Legendre polynomials with penalty scheme is developed for numerically modeling electromagnetic wave scattering problems. The primary aim of the proposed method is to more accurately analyzing scattering and coupling problems in plasmonics, in which optical waves interact with nanometer-sized metallic structures. Using light scattering by a silver circular cylinder as a first example, the formulated method is demonstrated to achieve numerical accuracy in near-field calculations on the order of 10^{-9} with respect to a unity field strength of the incident wave with excellent exponentially convergent behavior in numerical accuracy. Then, scattering by a dielectric square cylinder and that by several coupled metallic structures involving circular cylinders, square cylinders, or dielectric coated cylinders are examined to provide high-accuracy coupled near-field results.**

***Index Terms*—Electromagnetic near fields, electromagnetic wave scattering, plasmonics, pseudospectral frequency-domain (PSFD) method.**

I. Introduction

PLASMONICS is a relatively new field concerning the collective electromagnetic resonances of free electrons inside nanometer-scaled metallic structures [1], which has been widely studied and applied in many areas, like surface enhanced Raman scattering (SERS) [2], nanoantennas [3], waveguides [4], etc. Strong electromagnetic fields can be locally enhanced and radiated by this collective oscillation of electric charges. The field coupling between metallic nanoparticles under different incident polarizations thus plays an important role in such plasmonics research. Accurate electromagnetic near-field calculation is essential and significant for understanding the underlying optical behaviors [5]. However, due to the nanometer-sized dimension and spacing of metallic particles as well as strongly enhanced near fields, there exist challenges to achieve relevant numerical simulations with good accuracy. The Mie theory [6] and the multiple scattering methods [7], [8] for analytically calculating light wave scattering by spheres or circular cylinders have been proposed. But for more general geometries of the plasmonic objects, numerical methods, like the finite-difference time-domain (FDTD) method [9], [10] and the finite element method (FEM) [11], [12], could provide more flexibilities. Plasmon resonance and field enhancement in complicated structures have also been analyzed using the surface integral method [13] and the volume integral method [14] and discussed by the surface-charge hybridization picture [15].

To more accurately model the interaction of electromagnetic waves with metallic structures, we present here a new Legendre pseudospectral frequency-domain (PSFD) method to solve Maxwell's equations for relevant two-dimensional (2-D) scattering problems. Although not so popularly used, the pseudospectral methods have been demonstrated their high-order accuracy and fast convergence behavior in applications to computational electromagnetics in time domain [16]–[19]. The idea of the pseudospectral method in frequency domain was initially proposed by Liu [20] based on Chebyshev polynomials and the second-order Helmholtz equation to solve a scattering problem. Later, based on Helmholtz equations, pseudospectral eigenmode solvers have been established for analyzing 2-D photonic crystals [21] and obtaining full-vector optical waveguide modes [22]. In this paper, we formulate our new PSFD method, instead, from the first-order differential equations using the similar scheme of a related Legendre pseudospectral time-domain (PSTD) method recently established [23] and utilizing the Legendre polynomials as the interpolation basis. Besides, the penalty scheme as developed in [23] is used to better handle boundary conditions for well-posedness consideration, and the perfectly matched layers (PMLs) [24]–[26]

Manuscript received February 04, 2012; revised November 11, 2012, November 23, 2012; accepted November 26, 2012. Date of publication December 12, 2012; date of current version January 23, 2013. This work was supported in part by the National Science Council of the Republic of China under Grant NSC99-2628-M-002-008, Grant NSC99-2221-E-002-107-MY2, Grant NSC99-2115-M-009-012-MY3, and Grant NSC 101-2811-M-009-040, in part by the Excellent Research Projects of National Taiwan University under Grant 10R80919-1, and in part by the Ministry of Education of the Republic of China under "The Aim of Top University Plan" Grant.

C.-Y. Wang, S.-Y. Chung, and C.-P. Chen are with the Graduate Institute of Electronics Engineering and the Department of Electrical Engineering, National Taiwan University, Taipei 10617, Taiwan.

C.-H. Teng is with the Department of Applied Mathematics and Center of Mathematical Modeling and Scientific Computing, National Chiao Tung University, Hsinchu 30010, Taiwan.

J.-K. Wang is with the Institute of Atomic and Molecular Sciences, Academia Sinica, and the Center for Condensed Matter Sciences, National Taiwan University, Taipei 10617, Taiwan.

H. Chang is with the Department of Electrical Engineering, the Graduate Institute of Photonics and Optoelectronics, and the Graduate Institute of Communication Engineering, National Taiwan University, Taipei 10617, Taiwan (e-mail: hcchang@cc.ee.ntu.edu.tw).

Digital Object Identifier 10.1109/JLT.2012.2233714

are incorporated into the PSFD formulation to absorb outward propagating waves and effectively reduce reflection of out-going waves. The multidomain approach is employed, as in [23], with which the computational domain with the PMLs is divided into suitable number of subdomains, with the material interfaces fitting the sides of some subdomains, so that the field continuity conditions can be accurately fulfilled. The equations approximating the physical processes of the corresponding subdomains are finally packed into a linear matrix equation which can be easily solved by iterative algorithms. Using the PSFD method, we will show that numerical accuracy on the order of 10^{-9} can be achieved in the scattered-field calculation of a circular metallic cylinder, as compared with known analytical results provided in [27], [28]. More importantly, this PSFD method provides exponentially convergent rate in numerical accuracy with respect to grid resolution, which implies its efficiency in that few grid points added can exponentially increase computation accuracy. We believe this method can provide high-accuracy results in the analysis of electromagnetic field characteristics of plasmonic problems including the important ones of coupled cylinder structures.

The finite-difference time-domain (FDTD) method [9] has been a popular numerical analysis and simulation method in computational electromagnetics, including plasmonics. For curved material interfaces, the simple stair-casing approximation of such interfaces as often utilized in the FDTD calculation of the electromagnetic field may result in numerical-accuracy reduction in field values along the curved interface [29]. However, obtaining high-accuracy near fields for such situations can be important for understanding the plasmonic phenomenon and proposing relevant applications. More efforts must be paid for overcoming such stair-casing problem in the FDTD method, e.g., using the conformal scheme [30], the triangular mesh [31], the effective permittivity [32], etc. The PSFD method, however, can avoid such stair-casing problem since its subdomain partitioning with curvilinear geometries can match exactly to the shape of the structure interface [33], thus can provide accurate computation.

Furthermore, in numerically modeling the plasmonic structures, material dispersive properties of metals need to be carefully considered. In time-domain computation methods, the auxiliary differential equation (ADE) technique [9] can be employed to take into account the Drude-Lorentz material model for a metal in the simulation. But the parameters in the material dispersion model need to be carefully assigned through curve fitting the measured dielectric function of the metal [34], [35]. As a frequency-domain method, however, the PSFD method can directly adopt the measured or given complex dielectric constant of the metal at the considered frequency without needing the ADE approach and the associated curve-fitting procedure for treating material dispersion in the electromagnetic calculations.

The remainder of this paper is outlined as follows. Maxwell's equations with the penalty scheme for the 2-D scattering problem are described in Section II. The Legendre pseudospectral method is introduced in Section III. Scattering calculation results for a silver circular cylinder, a dielectric square cylinder, and several coupled metallic structures involving circular cylinders, square cylinders, or dielectric coated cylinders are presented and discussed in Section IV. Some remarks on the proposed formulation and scheme are given in Section V. The conclusion is drawn in Section VI.

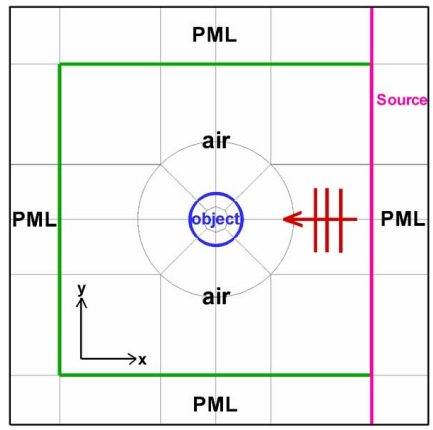

Fig. 1. Computational domain with pseudospectral subdomain division for the scenario in which a plane wave is scattered by a 2-D object.

II. Maxwell's Equations With the Penalty Scheme

For time-harmonic electromagnetic fields, $\mathbf{E}$ and $\mathbf{H}$, in a linear isotropic medium region with permittivity ε and permeability μ, Maxwell's curl equations can be written in the complex form as

$$-j\omega\mu\mathbf{H} - \nabla \times \mathbf{E} = \mathbf{M} \tag{1a}$$

$$-j\omega\epsilon\mathbf{E} + \nabla \times \mathbf{H} = \mathbf{J} \tag{1b}$$

where $\mathbf{J}$ and $\mathbf{M}$ represent the source electric and magnetic current densities, respectively, and ω is the angular frequency. Here, we consider the 2-D problem with no field variation along the z direction. Fig. 1 shows one example scenario in which a plane wave is scattered by a 2-D circular cylinder. We particularly study the transverse-magnetic (TM) waves with E_x, E_y, and H_z field components because of plasmonics applications. Therefore, Maxwell's curl equations become three first-order equations as

$$-\frac{\partial H_z}{\partial y} - j\omega\epsilon E_x = J_x \tag{2a}$$

$$-\frac{\partial H_z}{\partial x} - j\omega\epsilon E_y = J_y \tag{2b}$$

$$\frac{\partial E_x}{\partial y} - \frac{\partial E_y}{\partial x} - j\omega\mu H_z = M_z. \tag{2c}$$

In the multidomain PSFD method, the computational domain is partitioned into suitable non-overlapping subdomains of curvilinear quadrilateral shape. Using the scattering by a circular cylinder as depicted in Fig. 1 as an example, if boundary conditions are rigorously considered at the interface between adjacent subdomains I and II with the unit normal vector perpendicular to the interface expressed as $\hat{n} = n_x\hat{x} + n_y\hat{y}$, the continuity of tangential fields across the interface for source-free dielectrics requires that

$$H_z^I = H_z^{II} \tag{3a}$$

$$E_t^I = E_t^{II} \tag{3b}$$

for the TM waves, where the superscripts, I and II, denote the subdomains and E_t denotes the tangential electric field, i.e., $E_t = n_y E_x - n_x E_y$.

In our formulation, an incident TM plane wave is generated by assigning a uniform y-directed source surface current density $\mathbf{J_s}$ with unit A/m on the PML/air interface, as shown in Fig. 1, using the required boundary condition, $\hat{n} \times (\mathbf{H}^I - \mathbf{H}^{II}) = \mathbf{J_s}$, where I and II refer to the corresponding PML subdomain and air subdomain, respectively, and M_z is taken to be zero in (2c). This y-directed $\mathbf{J_s}$ would generate both y-polarized rightward (to the PML) and leftward propagating plane waves [36], with the rightward wave absorbed by the PML. Note that the relation between $\mathbf{J_s}$ and $\mathbf{J}$, the latter being the volume current density with unit A/m^2, is $\mathbf{J_s} = \int \mathbf{J} dx$ if $\mathbf{J_s}$ flows in the y direction, and we would have $\mathbf{J} = \mathbf{J_s}/\omega_0$, where ω_0 is the quadrature weight on the interface which will be defined in the next section.

In [23], the Legendre PSTD formulation with the penalty scheme based on well-posed boundary impositions of physical boundary conditions in terms of characteristic variables has been discussed in detail. The same penalty scheme is employed here to impose weakly characteristic boundary conditions. Briefly speaking, (2) can be first written as

$$j\omega M q + A_x \frac{\partial q}{\partial x} + A_y \frac{\partial q}{\partial y} = J_{\text{current}} \tag{4}$$

where $q = [E_x, E_y, H_z]^T$, $M = -\text{diag}[\epsilon, \epsilon, \mu]$, and the matrices A_x and A_y are simply constructed with 0, 1, and -1 corresponding to the presence of fields in (2). Next, the penalty term $P = (\delta/\omega_0) S(n) \Lambda [R(n) - R^{BC}(n)]$ will be added. The matrices, Λ and $S(n)$, are constructed respectively from the eigenvalues and eigenvectors of the matrix $A(n)$, which is defined as $A(n) = n_x A_x + n_y A_y$, and the characteristic state vectors $R(n)$ are defined as $R(n) = S^T(n) q$ as in [23]. Then, after matrix multiplications of $S(n)$, Λ, and $[R(n) - R^{BC}(n)]$ in the penalty term P, Maxwell's equations in (2) with penalty $(\tau/2)P$ added become

$$-j\omega\epsilon E_x^I + \frac{\partial H_z^I}{\partial y} - \frac{\tau}{2}\frac{\delta}{\omega_0} n_y^I \left(H_z^I - H_z^{II}\right) = J_x \tag{5a}$$

$$-j\omega\epsilon E_y^I - \frac{\partial H_z^I}{\partial x} + \frac{\tau}{2}\frac{\delta}{\omega_0} n_x^I \left(H_z^I - H_z^{II}\right) = J_y \tag{5b}$$

$$-j\omega\mu H_z^I + \frac{\partial E_x^I}{\partial y} - \frac{\partial E_y^I}{\partial x} - \frac{\tau}{2}\frac{\delta}{\omega_0} n_y^I \left(E_x^I - E_x^{II}\right) + \frac{\tau}{2}\frac{\delta}{\omega_0} n_x^I \left(E_y^I - E_y^{II}\right) = M_z \tag{5c}$$

where δ is unity when the grid point is on the boundary edge, and is zero otherwise [23]. The variable τ is a free parameter defined by Theorem 3.1 in [23] with value $\tau \geq 1$ for supporting (5) to be a convergent system during iteration processes. In the PML subdomains, (5) are rewritten, following the derivations in [23] and [26], as

$$-j\omega\epsilon E_x^I + (2\sigma_y - j\sigma_y^2)\omega\epsilon E_x^I + \frac{\partial H_z^I}{\partial y} - \frac{\tau}{2}\frac{\delta}{\omega_0} n_y^I \left(H_z^I - H_z^{II}\right) = J_x \tag{6a}$$

$$-j\omega\epsilon E_y^I - (2\sigma_x - j\sigma_x^2)\omega\epsilon E_y^I - \frac{\partial H_z^I}{\partial x} + \frac{\tau}{2}\frac{\delta}{\omega_0} n_x^I \left(H_z^I - H_z^{II}\right) = J_y \tag{6b}$$

$$-j\omega\mu H_z^I + \frac{\sigma_y'}{j\omega + \sigma_y} E_x^I - \frac{\sigma_x'}{j\omega + \sigma_x} E_y^I + \frac{\partial E_x^I}{\partial y} - \frac{\partial E_y^I}{\partial x} - \frac{\tau}{2}\frac{\delta}{\omega_0} n_y^I (E_x^I - E_x^{II}) + \frac{\tau}{2}\frac{\delta}{\omega_0} n_x^I \left(E_y^I - E_y^{II}\right) = M_z \tag{6c}$$

where σ_x and σ_y are absorbing profiles along the x and y axes, respectively, and σ_i' denotes the derivative of σ_i with respect to i $(i = x, y)$. Taking σ_x as an example, we choose $\sigma_x = \kappa(|x - x_0|/L_{\text{PML}})^m$, where $|x - x_0|$ is the distance of the point, x, from the initial point, x_0, L_{PML} is the total length of PML, and the parameters κ and m are free variables for tuning the PML performance. After employing the Legendre pseudospectral scheme and packing all subdomains, (5) and (6) would lead to a linear matrix equation, $AX = B$, with the unknown vector X consisting of $\mathbf{E}$ and $\mathbf{H}$ fields, the vector B corresponding to the known sources, and the A matrix consisting of spatial differential operators and penalty terms. The unknown electric and magnetic fields can be solved from $X = A^{-1}B$ using efficient iterative algorithms such as the bi-conjugate gradient (BiCG) method.

III. Legendre Pseudospectral Method

Now, we discuss the Legendre pseudospectral method for numerically treating the spatial derivatives in the above governing equations. Under the multidomain scheme, each curvilinear quadrilateral subdomain region in Cartesian coordinates (x, y) can be mapped onto a square region $[-1, 1] \times [-1, 1]$ in curvilinear coordinates (ξ, η) by using the transfinite blending function described in [29] to construct $\xi = \xi(x, y)$ and $\eta = \eta(x, y)$. Applying the chain rule, derivatives of a 2-D function $f(x, y)$ will then become

$$\frac{\partial f(x,y)}{\partial x} = \frac{\partial \xi}{\partial x}\frac{\partial f(x,y)}{\partial \xi} + \frac{\partial \eta}{\partial x}\frac{\partial f(x,y)}{\partial \eta} \tag{7a}$$

$$\frac{\partial f(x,y)}{\partial y} = \frac{\partial \xi}{\partial y}\frac{\partial f(x,y)}{\partial \xi} + \frac{\partial \eta}{\partial y}\frac{\partial f(x,y)}{\partial \eta}. \tag{7b}$$

Some properties of Legendre polynomials, which we use as the basis for the interpolation of a function, will be given below.

In the Legendre pseudospectral method, spatial arrangement of grid points is defined by the Legendre–Gauss–Lobatto (LGL) quadrature points ξ_i arranged in the interval $[-1, 1]$, which are the roots of the polynomial $(1 - \xi^2) P_N'(\xi)$ [23] with the prime denoting derivative and P_N being the Legendre polynomial of degree N defined by

$$P_N(\xi) = \frac{1}{2^N N!}\frac{d^N}{d\xi^N}(\xi^2 - 1)^N .. \tag{8}$$

Associated with these LGL quadrature points are a set of quadrature weights ω_i for $i = 0, 1, 2, \ldots, N$. If $f(\xi)$ is a

polynomial of degree at most $2N+1$, we have the quadrature rule [23]

$$\sum_{i=0}^{N} f(\xi_i)\omega_i = \int_{-1}^{1} f(\xi)d\xi \tag{9}$$

where the quadrature weights are defined by

$$\omega_i = \begin{cases} \frac{2}{N(N+1)}, & i = 0, N \\ -\frac{2}{(N+1)}\frac{1}{P_N(\xi_i)P'_{N-1}(\xi_i)}, & \text{otherwise.} \end{cases} \tag{10}$$

Based on these LGL collocation points, one can use the degree-N Lagrange interpolation polynomials $l_j(\xi)$ as the bases to approximate an arbitrary function $f(\xi)$ such that

$$f(\xi) \approx \sum_{j=0}^{N} f(\xi_j) l_j(\xi) \tag{11}$$

where

$$l_j(\xi) = -\frac{(1-\xi^2)P'_N(\xi)}{N(N+1)(\xi-\xi_j)P_N(\xi_j)}. \tag{12}$$

Then, the derivative of the function $f(\xi)$ at the LGL quadrature point ξ_i can also be approximated as

$$\frac{df(\xi_i)}{d\xi} \approx \sum_{j=0}^{N} \frac{dl_j(\xi_i)}{d\xi} f(\xi_j) = \sum_{j=0}^{N} D_{ij} f(\xi_j). \tag{13}$$

The differential coefficient D_{ij} is defined in [23] by

$$D_{ij} = \begin{cases} -\frac{N(N+1)}{4}, & i = 0 \\ \frac{N(N+1)}{4}, & i = N \\ 0, & \text{otherwise} \end{cases} \tag{14}$$

if $i = j$; and

$$D_{ij} = \frac{P_N(\xi_i)}{P_N(\xi_j)} \frac{1}{\xi_i - \xi_j} \tag{15}$$

if $i \neq j$. The so-called differential matrix operator with D_{ij} elements can thus be substituted into the spatial derivative in (13) as

$$\frac{\partial}{\partial \xi} = \begin{bmatrix} D_{00} & D_{01} & \cdots & D_{0N} \\ D_{10} & D_{11} & \cdots & D_{1N} \\ \vdots & \vdots & \vdots & \vdots \\ D_{N0} & D_{N1} & \cdots & D_{NN} \end{bmatrix}. \tag{16}$$

This is the key feature of the Legendre PSFD method, i.e., for the 1-D example, the derivative of $f(\xi)$ at an LGL point ξ_i in the region $[-1, 1]$ can be approximated in terms of $f(\xi)$ values at the $N+1$ LGL points in the same region. Spatial derivatives of fields in (5)–(7) can be simply replaced by these differential matrix operators D_{ij} in the linear matrix system. The matrix A thus becomes a sparse matrix containing penalty, PML, and D_{ij} terms. Note that those D_{ij} terms for spatial derivatives repeatedly appear in A and are located with regularity, thus only this small D matrix in (16) is needed to be stored and our PSFD implementation will be memory-saving, which can then be applied to solve large problems or those requiring dense grid points. In Fig. 2, the grid meshes based on the LGL points in each subdomain, except the PML ones, are plotted for $N = 12$. As shown in the figure, the curved structure and the whole computational region are partitioned into curvilinear subdomains, and $(N+1)\times(N+1)$ LGL grid points are not uniformly distributed but somewhat following the outline of the domain edges. Please note that the LGL grid points at each edge side of a subdomain are colocated with the LGL grid points at one edge side of its adjacent subdomain. These colocated grid points are counted as distinct sets of points, and the penalty scheme is applied on the two sets for exchanging information of boundary conditions.

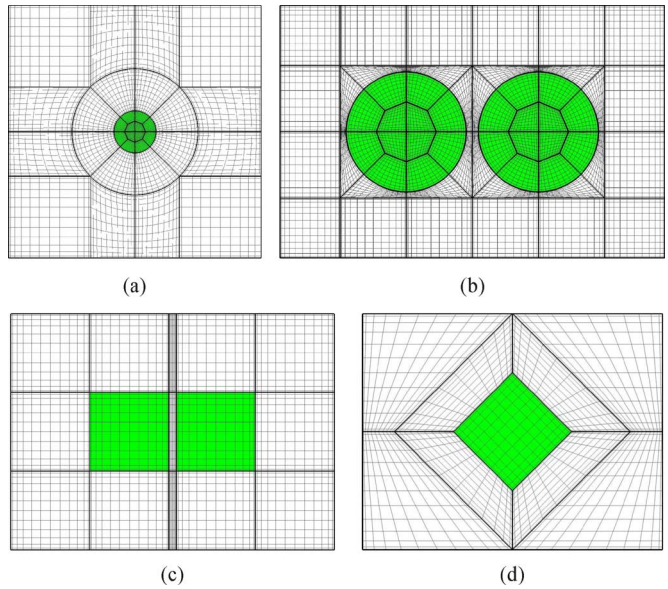

Fig. 2. Portion of the subdomain division profile in the computational domain near the cylinder scatterers (the colored region) for $N = 12$. (a) A single circular cylinder. (b) Two coupled circular cylinders. (c) Two coupled rectangular cylinders. (d) 45°-tilted square cylinder.

IV. Numerical Results

Here, the PSFD method is applied to analyze some basic scattering problems. Accuracy will be first verified by examining a circular-metallic-cylinder problem and comparing the results with those obtained from the analytical approach. With the high accuracy provided, the PSFD method is then applied to simulate several coupled structures between closely placed, in nanometer scale, metallic cylinders and investigate their optical behaviors.

A. Single Circular Metallic Cylinder

First, we examine the accuracy of the formulated Legendre PSFD method by solving a simple problem of TM scattering of a plane wave by a silver circular cylinder in free space at an optical wavelength. Such problem is known to have an analytical solution [27], [28]. Nevertheless, it is a good example to test how accurate a numerical analysis method can perform when dealing with plasmonic structures. The computational-domain setup with PMLs and the subdomain division is as shown in Fig. 1, and the grid mesh is as depicted in Fig. 2(a). The radius of the cylinder is $R = 0.25$ μm and the wavelength of the incident plane wave is $\lambda = 1$ μm. At this wavelength, the

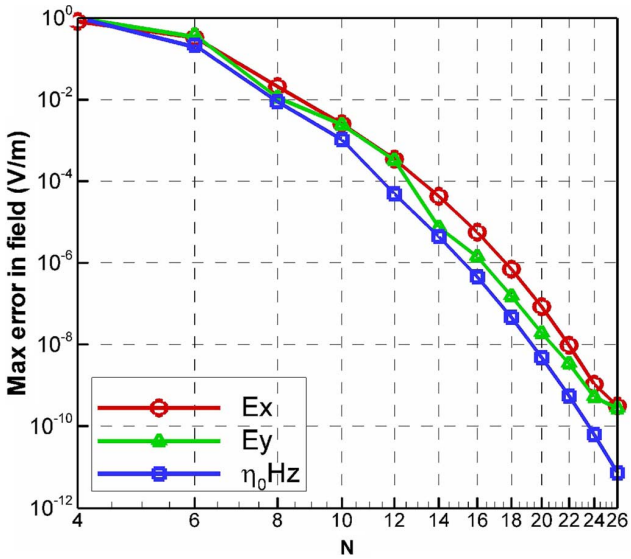

Fig. 3. Maximum absolute difference between the PSFD calculated field value and its corresponding analytical one scanned over the computational domain versus the degree of the Legendre polynomial used for the E_x, E_y, and H_z components, respectively, for TM scattering of a plane light wave at $\lambda = 1$ μm by a silver circular cylinder of radius 0.25 μm in free space.

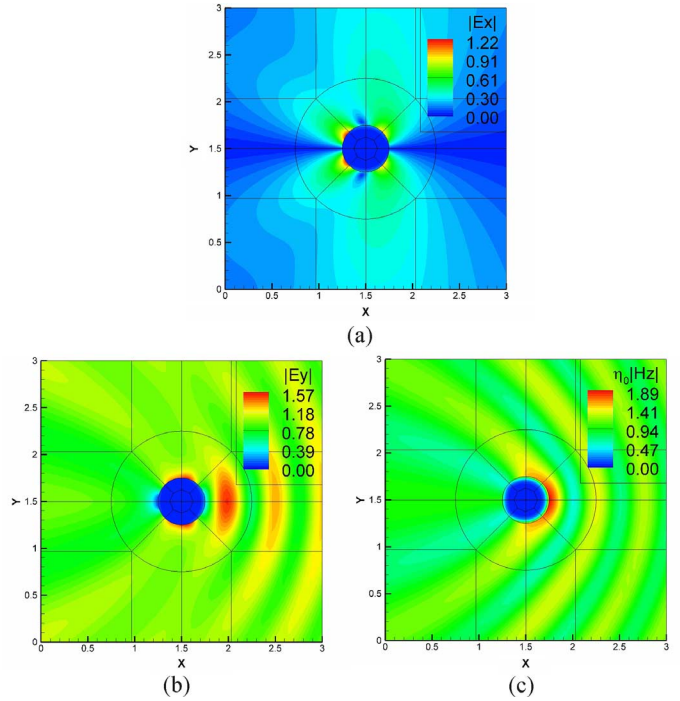

Fig. 4. Field profiles for (a) $|E_x|$, (b) $|E_y|$, and (c) $|H_z|$, respectively, for the case of Fig. 3, with the incident wave propagating from right to left.

measured complex dielectric constant of silver is about $\varepsilon_r = -50.981 + i0.562$ [34]. Fig. 3 shows the maximum absolute difference, $|\Delta q|$, between the PSFD calculated field value and its corresponding analytical one scanned over the computational domain versus the degree N of the Legendre polynomial used for the E_x, E_y, and H_z components, respectively, when the incident electric field intensity is 1 V/m, where q refers to the field component. For H_z, the difference in $\eta_0 H_z$ is considered, where η_0 is the free-space impedance. It is seen that the errors are on the order of 10^{-2} when $N = 8$ and on the order of 10^{-4} when $N = 12$ and can get down to 10^{-9} when $N > 22$. These results demonstrate that our PSFD algorithm can provide high accuracy for solving light scattering by plasmonic structures. Also, the convergent plots show that the error exponentially, rather than linearly, decreases with respect to N. This is the inherent characteristic of the spectral method having the convergent ratio proportional to $(\Delta x)^N \sim (1/N)^N$. Fig. 4(a)–(c) plots the field profiles for $|E_x|$, $|E_y|$, and $\eta_0|H_z|$, respectively, when the incident TM wave comes from right with $|E_y|$ polarization. The computing resources used are described as follows. For $N = 6, 8, 10$, and 12, the required matrix sizes are 31 164, 51 516, 76 956, and 107 484, respectively, the computer running times are 175, 429, 958, and 1970 s, respectively, and the memory usages are 9, 14, 20, and 27 Mb, respectively, executed by a single processing core on a personal computer with quad-core i7 3.42-GHz CPU in Linux environment. The computation time approximately doubles as N is increased by two, and the memory usages are not much. Note that the accuracy with $N = 12$ can be more than what is required in practice since the error in the calculated field is on the order of 10^{-4} as mentioned above.

In this verifying example of the PSFD method achieving such high accuracy, PML tuning is also an important process. From the given absorbing profile σ of PML, free parameters κ and m can be varied to optimize the accuracy. According to our experiences and in this case, the choices of $20 \leq \kappa \leq 30$ and $m = 2$ or 3 can provide better results as shown. This gives a gradually growing profile, and we adopt a wide PML with 3-μm thickness for reducing reflection of waves.

B. The Single Dielectric Square Cylinder

Scattering of a 45°-tilted dielectric square cylinder investigated in [37] is considered next. The side length of the square is $d = 3.5/k$, where $k = 2\pi/\lambda_0$ is the free-space wavenumber, and the plane wave incidence is as indicated in the inset of Fig. 5 with wavelength λ_0. Here, the dimensions are all normalized to k according to [37], so the size of the dielectric cylinder is measured in terms of $\lambda_0/(2\pi)$. Note that the square was assumed in [37] to have rounded corners with a radius of curvature $\rho = 0.01/k$ but it is assumed to have sharp corners in our calculations. Thus, there would be four singular points expected at these sharp corners in our results. The tangential electric field of the TM case versus kS, where S is the distance along the upper square surface from the left apex to the right apex, is shown in Fig. 5(a) and (b) for cylinders of dielectric constants $\varepsilon_r = 2.5$ and $\varepsilon_r = 10$, respectively. The calculations were done for N from 12 up to 28. The results are seen to well agree with those of [37], even for smaller Ns. Notice that the fields at the singular points, $kS = 3.5$ for example, grow up as the grid resolution (or N) increases. Here, we used only one subdomain for this square structure, and there are $2 \times (N + 1)$ points along $kS = 0$ to $kS = 7$. The field distributions with $\varepsilon_r = 10$ are depicted in Fig. 6. Because the incident wave comes from the left, the fields are seen to be longitudinally symmetric. The singular points can be observed at the upper and bottom apexes in Fig. 6(b). To observe more clearly the singular-point characteristics, the expanded view of those results in Fig. 5(a) near $kS = 3.5$ is shown in Fig. 5(c). Note that, at $kS = 3.5$, there

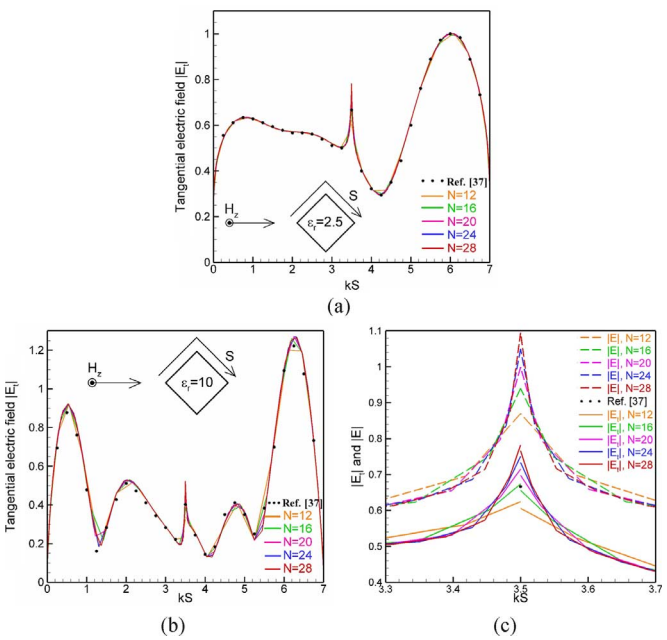

Fig. 5. Tangential electric field ($|E_t|$) versus kS ($k = 2\pi/\lambda_0$) for (a) $\varepsilon_r = 2.5$ and (b) $\varepsilon_r = 10$ for the scattering of a 45°-tilted dielectric square cylinder with side length $d = 3.5/k$. The dots are adopted from [37] and other lines stand for PSFD calculated results of different degrees (N). (c) The expanded view of those results in (a) near $kS = 3.5$ together with the corresponding PSFD calculated total electric field ($|E|$) results for showing the singular electric-field characteristic at the dielectric corners.

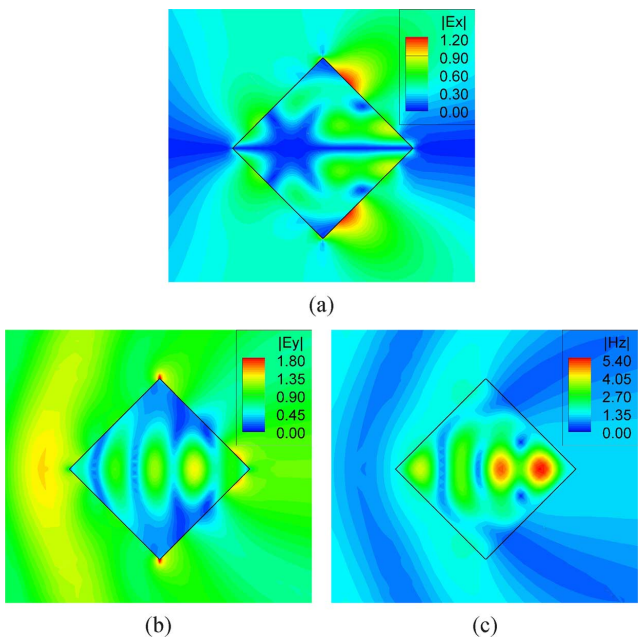

Fig. 6. Field profiles for (a) $|E_x|$, (b) $|E_y|$, and (c) $|H_z|$, respectively, for the case of Fig. 5(b).

are two $|E_t|$ values for each N since the tangential component value referring to the left side and that referring to the right side are different. Also displayed in Fig. 5(c) are the corresponding profiles for the magnitudes of the total electric field, $|E|$, which show sharper singular behavior. The subdomain division profile near the square cylinder is plotted in Fig. 2(d).

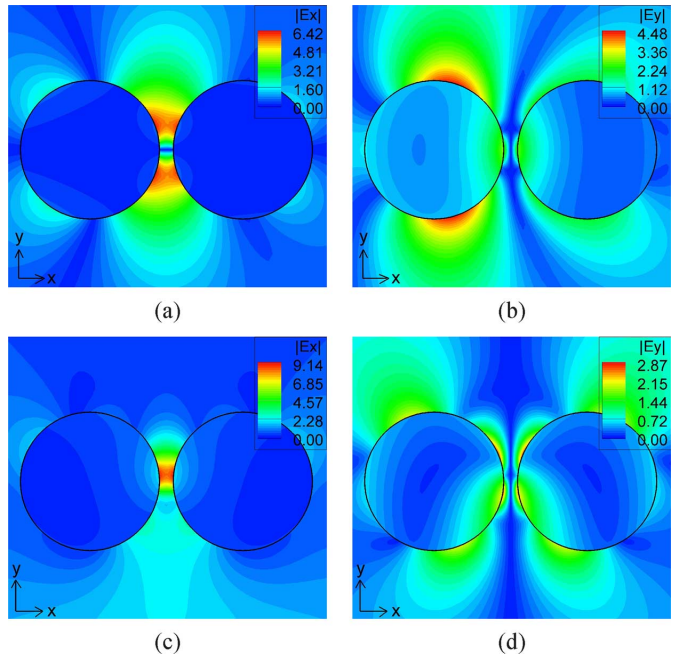

Fig. 7. $|E_x|$ and $|E_y|$ field distributions for plane-wave scattering by two coupled silver circular cylinders. The plane wave is incident from left in (a) and (b), and from bottom in (c) and (d). The radii are 50 nm and the side spacing between the two cylinders is 10 nm.

C. Two Coupled Circular Metallic Cylinders

The field coupling between metallic nanoparticles plays an important role in plasmonic research, which in particular may result in strong local-field enhancement that can provide many useful applications. We apply the PSFD method to study the phenomenon of field coupling between two silver nano-cylinders, with focus on two closely placed cylinders interacting with incident light waves of different directions and polarizations.

The first case is a system of two 50-nm-radius circular cylinders with 10-nm spacing allocated along the x-axis. For the $|E_x|$ and $|E_y|$ distribution results shown in Fig. 7(a) and (b), the wave is incident from left at $\lambda = 0.421$ μm and with E_y polarization. The measured complex dielectric constant of silver at this wavelength is $-5.598 + i0.213$. The two cylinders are coupled such that strong electric field enhancement occurs within the gap between them, with the maximum $|E_x|$ being about 6.42 times the incident electric field intensity, as indicated in the color bar in Fig. 7(a). Due to the direction of the incident wave, the electric field profile is longitudinally symmetric with respect to the arrangement of cylinders. There is a null at the center, and the fields below and above it are oppositely signed in phase. Also, the incident E_y polarization causes the first cylinder to oscillate with strong E_y fields on both y-ended surfaces, as depicted in Fig. 7(b), and less influence is on the second cylinder due to the shielding from the first cylinder.

If the propagation direction of the incident wave is changed to be bottom-up with E_x polarization, strong field enhancement occurs at $\lambda = 0.4$ μm with the $|E_x|$ and $|E_y|$ field distributions shown in Fig. 7(c) and (d), respectively. At this wavelength, the measured complex dielectric constant of silver is about $-4.435 + i0.211$. In this case, obviously, the incident E_x field leads the free electrons in both cylinders to oscillate horizontally and induces a strongly coupled E_x field within the gap,

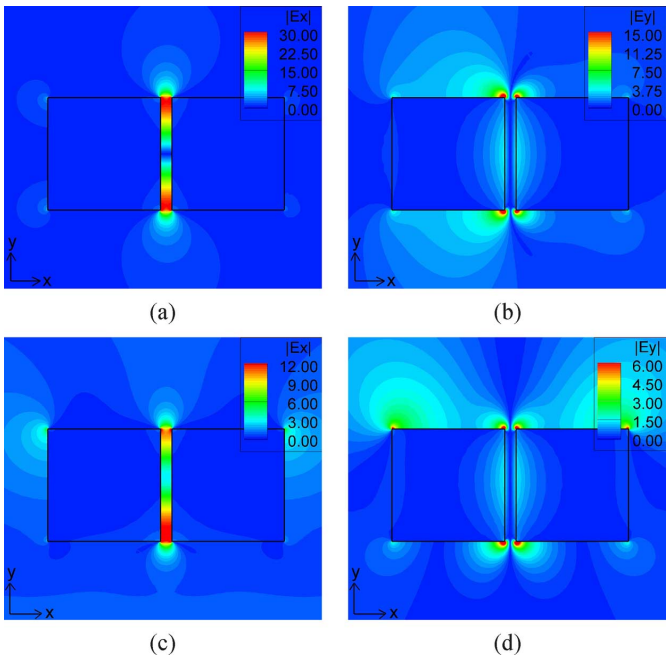

Fig. 8. $|E_x|$ and $|E_y|$ field distributions for plane-wave scattering by two coupled silver rectangular cylinders. The plane wave is incident from left in (a) and (b), and from bottom in (c) and (d). The edge length are 100 nm and the side spacing between the two cylinders is 10 nm.

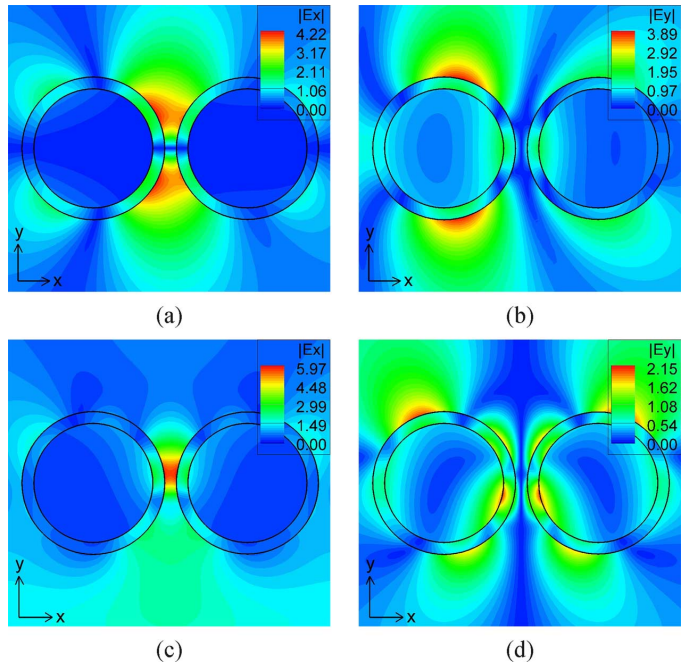

Fig. 9. $|E_x|$ and $|E_y|$ field distributions for plane-wave scattering by two coupled silver circular cylinders having a dielectric coating of 10-nm thickness. The plane wave is incident from left in (a) and (b), and from bottom in (c) and (d).

which is about 9.14 times enhancement. Note that the maximum induced E_x field is not exactly located right at the center, but about 5 nm upper. The induced E_y field is transversely symmetric and not strongly enhanced, and the E_y phases of the two cylinders are reversed such that there also exists a null in between. It is seen in the above two situations that the plane wave incident from the bottom provides higher field enhancement than that from the left.

D. Two Coupled Square Metallic Cylinders

Next, we study the field coupling between two square metallic cylinders. Different from the circular ones, the square cylinders have four sharp corners, which would cause singular points and thus induce extremely, infinity theoretically, strong fields would exist around these apexes, causing challenges in numerical computations.

The simulated case is a system of two square cylinders, each having 100-nm edge width, again with 10-nm spacing. This structure is to be compared with the above one of circular cylinders. Fig. 8(a) and (b) shows the $|E_x|$ and $|E_y|$ distributions when the wave is incident from left at $\lambda = 0.627$ μm. The complex dielectric constant of silver at this wavelength is about $-17.98 + i0.485$. From the $|E_x|$ field shown in Fig. 8(a), it reveals two spots of field enhancement at the upper and lower corners in the gap, with the field enhancement being as high as up to 30 times. The calculated fields at the apexes would be even higher as N is increased. As in the case of coupled circular cylinders, the $|E_y|$ profile is distributed mainly at both y-ended edges of the first cylinder. The appearance of symmetric upper and lower field-enhancement regions is quite similar to those in Fig. 7(a) and (b).

Likewise, if we change the incident wave direction to bottom-up at $\lambda = 0.613$ μm, the strong $|E_x|$ enhancement appears in the gap near the bottom corner, as shown in Fig. 8(c), due to the x-polarized incident field, with the enhancement being up to 12 times, which is smaller than that in Fig. 8(a). The complex dielectric constant of silver at this wavelength is $-16.96 + i0.485$. Note that the field is now not enhanced at the center but near the bottom of the gap. Opposite field phases in Fig. 8(a) with respect to horizontal symmetric plane and in Fig. 8(d) with respect to the vertical symmetric plane in Fig. 8(d) cause obvious null-field appearances within the gap region.

E. Two Coupled Metallic Cylinders With Dielectric Coating

We further study the situations with each of the cylinders in Figs. 7 and 8 coated with a 10-nm-thickness dielectric layer of dielectric constant $\varepsilon_r = 3$. We maintain the diameter or edge width of each silver cylinder, and the gap size is still kept as 10 nm. It is known that this outer dielectric material can make the plasmonic resonant frequency shifted, but the optical field characteristics are rarely seen, especially for coupled cylinders. The results corresponding to Fig. 7 are shown in Fig. 9 and those corresponding to Fig. 8 are shown in Fig. 10. The incident wavelengths in Fig. 9(a)–(b), Fig. 9(c)–(d), and Fig. 10(a)–(b), and Fig. 10(c)–(d) are 0.467, 0.417, 0.649, and 0.616 μm, respectively, with the corresponding complex dielectric constants of $-7.97+i0.270$, $-5.42+i0.219$, $-19.42+i0.46$, and $-17.193+i0.496$, respectively. The characteristics of $|E_x|$ and $|E_y|$ profiles are seen to be quite similar with those in Figs. 7 and 8, but the localized fields now appear mainly at the dielectric-dielectric interfaces and in the gaps, which could reduce the ohmic losses in the metals. The field enhancement is found to be lower compared with uncoated cases, which can be explained by the

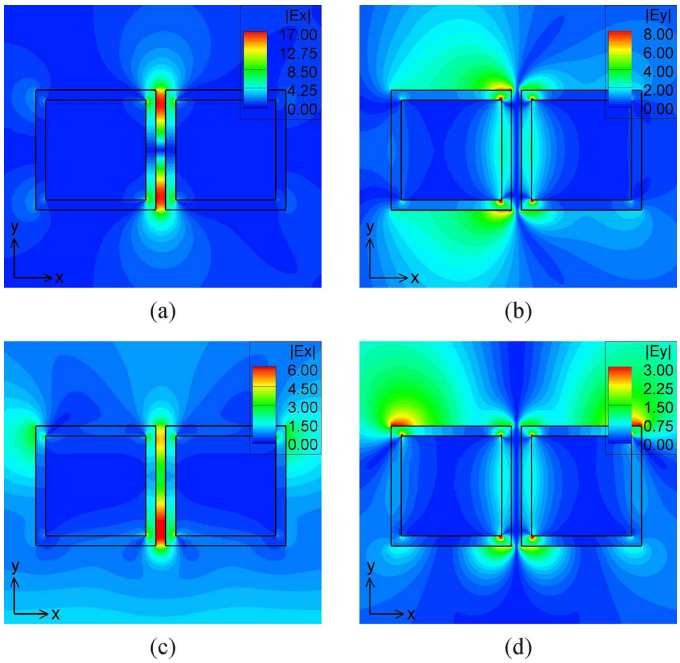

Fig. 10. $|E_x|$ and $|E_y|$ field distributions for plane-wave scattering by two coupled silver rectangular cylinders having a dielectric coating of 10-nm thickness. The plane wave is incident from left to right in (a) and (b) and from bottom in (c) and (d).

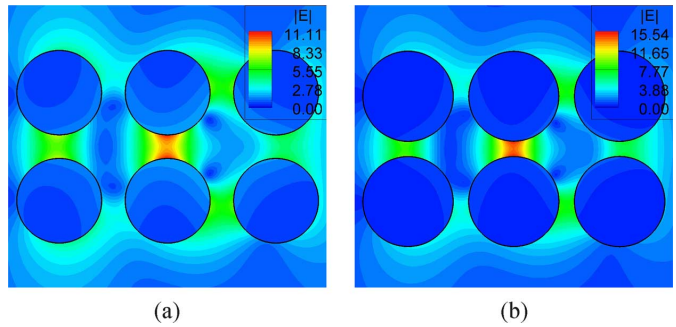

Fig. 11. $|E|$ field distributions for plane-wave scattering by six silver circular cylinders with incident wave from left. (a) Cylinder radius $R = 36$ nm at $\lambda = 460$ nm. (b) Cylinder radius $R = 58$ nm at $\lambda = 650$ nm. All gap widths are 20 nm.

fact that the actual distance between the metallic cylinders is 30 nm rather than 10 nm.

F. Three Pairs of Circular Metallic Cylinders

We finally investigate two-by-three arranged six-silver-cylinder arrays studied in [10], where the FDTD method was used for simulations. This cylinder arrangement is shown to give not only particle-particle but pair-pair interactions, thus strong localized field enhancement could be generated in the gap of the middle pair [10]. In [10], measured material characteristics for silver given in [35] instead of [34] were used. We also adopt the data in [35] in our calculations for comparison. Our PSFD results given in Fig. 11 are for the incident wave from left to right and the spacing between adjacent cylinders being 20 nm. In [10], it was found that with gap size of 20 nm and at $\lambda = 460$ nm, the maximum field enhancement of about 8.89 occurs when the cylinder radius is 36 nm. Our PSFD simulated $|E|$ profile for this case is shown in Fig. 11(a), where the maximum $|E|$ field value is 11.11 V/m, referring to the incident field of 1 V/m, and the field value at the center of the gap of the middle pair is about 9.33 V/m, which is larger than that value of [10] by 4.72%. The $|E|$ value is defined here by $|E| = (|E_x|^2 + |E_y|^2)^{1/2}$. The measured complex dielectric constant of silver given in [35] is about $\varepsilon_r = -6.53 + i0.737$ at this wavelength. If the value given in [34], $\varepsilon_r = -7.585 + i0.245$, is used, the PSFD calculated maximum $|E|$ field value and the field value at the center of the gap of the middle pair would be about 13.78 and 11.65 V/m, respectively.

When the wavelength is changed to 650 nm, the cylinder radius was found in [10] to be 58 nm for generating largest field enhancement of 13.04. Our results for this case are presented in Fig. 11(b), where the maximum $|E|$ field is 15.54 V/m and the field value at the same gap center is about 14.09 V/m, again larger than those values of [10] by 8.05%. The complex dielectric constant of silver cylinder is about $\varepsilon_r = -17.2 + i1.16$ from [35] for this incident wavelength. Again, if we choose to adopt the measured parameter from [34], which is $\varepsilon_r = -19.493 + i0.462$, the PSFD calculated maximum $|E|$ field value and the field value at the center of the gap of the middle pair would be about 17.07 V/m and 15.51 V/m, respectively.

V. Some Remarks on the Proposed Formulation and Scheme

The proposed pseudospectral formulation and scheme in this paper have been based on the Legendre collocation points, the first-order Maxwell's equations, and the penalty scheme for interface conditions, which are in contrast to some existing ones based on the Chebyshev collocation points, the second-order Helmholtz equations, and/or directly matching interface conditions. The advantages of our ones are discussed in the following.

A. Legendre Collocation Points Versus Chebyshev Collocation Points

A major factor, which makes the Chebyshev pseudospectral approximations based on the Chebyshev–Gauss–Lobatto points more popular than the Legendre pseudospectral approximations based on the Legendre–Gauss–Lobatto points, is the fast fourier transform (FFT). This technique allows the numerical derivatives to be computed in $N \log(N)$ operations. Indeed, Chebyshev pseudospectral method is very attractive for problems defined on regular domains, based on single domain computational framework. For these problems, either time-dependent or time-independent, if the required number of grid points is beyond 100, then the FFT technique does improve the computational efficiency. However, in a multidomain computational framework which can be used to solve problems defined on complicated domains, the number of grid points in each subdomain is generally much less than 100 and thus, we do not gain efficiency on using Chebyshev pseudospectral method [38]. Of course this does not mean we need to use Legendre pseudospectral method instead. The reason of using Legendre pseudospectral approximation will be discussed after addressing issues related to the penalty methodology of imposing boundary conditions.

B. Penalty Method for Interface Conditions and Directly Matching Interface Conditions

We now address issues related to the approaches of imposing boundary conditions. Generally speaking, an interface boundary condition is a constraint relating field values on both sides of the interface in a specific way, possibly involving differentiations and geometrical parameters. In the present study, the geometrical parameter is the unit vector normal to the interface. In a multidomain computational framework, a problem domain is decomposed into a union of subdomains. Thus, at the subdomain interfaces we need to enforce interface boundary conditions. As a consequence, it is necessary to specify a unique normal vector at every boundary grid point, and this becomes a problem at a vertex point of a 2-D subdomain. Is it possible to assign a unique normal vector at a vertex point? Or does it exist a unique normal vector at a vertex point? Frankly speaking, we have no answer to the problem and we doubt that there is an answer to the problem. Thus, this becomes a problem when we want to impose boundary condition through a directly matching approach at a location shared by vertex points of different subdomains, and great care must be exercised to resolve this issue. In contrast, the penalty methodology offers an edge-by-edge approach to impose boundary conditions [23], [39], [40]. It is not necessary to specify a unique normal vector at a vertex point, because a vertex point is an intersection of two boundary edges of a subdomain. Since we can specify normal vector functions along the edges of a subdomain, we define two normal vectors at a vertex point based on the normal vectors on the edges that intersect at the vertex. As a result, every vertex point is enforced with two penalty boundary conditions with field values from two attached edges belonging to different subdomains. This does not ruin the consistency (accuracy) of the scheme at all. As we have shown in our numerical experiments, the results are exponentially convergent. This explains why we adopt the penalty methodology for imposing boundary conditions.

C. Why the Legendre Pseudospectral Method?

The penalty method incorporates numerical partial differential equations and boundary conditions through a linear combination parameterized by a penalty parameter [23], [39]–[41]. The value of this parameter is commonly determined such that the scheme is stable in an energy sense. To conduct such an analysis, one needs to establish a discrete energy norm measurement. This issue makes Legendre pseudospectral method very attractive, because Legendre pseudospectral method is equipped with a quadrature integration rule (Legendre–Gauss–Lobatto quadrature rule) which can be used to construct a discrete L_2 norm measurement for grid-functions [42]. The Chebyshev pseudospectral method also has a quadrature integration rule [42]. However, the rule does not coincide with the usual L_2 energy norm measurements for functions. Using the Legendre–Gauss–Lobatto quadrature rule to conduct an energy estimate, one can determine the value of the penalty parameter to ensure the stability of a scheme in a theoretical basis, instead of a trial-and-error basis. This procedure is useful and important, because high-order accurate numerical methods, compared to the low-order accurate ones, are very sensitive to the impositions of boundary conditions [42], [43]. For time-dependent problems, if boundary conditions are not imposed properly, it often causes numerical blow-up solutions because of numerical instability inducing from subdomain boundaries. For time-independent or time-harmonic problems, improper impositions of boundary conditions may cause non-convergent solutions during iteration processes. Roughly speaking, these instabilities and nonconvergence problems are often resulting from numerical solution operators being unstable, in the sense that some eigenvalues of the solution operators have positive real part, commonly due to the impositions of boundary conditions. To avoid these unwanted situations, constructing a L_2 energy stable scheme in the theoretical stage becomes important in building a multidomain computational framework for simulations. Thus, based on the above arguments we adopt the Legendre pseudospectral method instead of the Chebyshev pseudospectral methods.

D. Why First-Order Maxwell's Equations Instead of Second-Order Helmholtz Equations?

In the present study, we solve first-order system Maxwell's equations instead of the equivalent second-order Helmholtz equations. This approach, indeed, is a drawback of the present formulation because it requires to solve more equations. In 2-D space, three coupled first-order partial differential equations need to be solved but only one equation to be solved if the problem is described by the second-order Helmholtz equation. However, the present first-order system formulation can be directly extended for waves in anisotropic media, even possibly with permittivity or permeability of media being a tensor. It is because the material parameters are not associated with the curl operator parts [23], [40]. Thus, we do not need to reformulate the penalty boundary condition formulations. As mentioned earlier, the penalty type boundary formulations avoid the ambiguity of specifying normal vectors at subdomain vertex points and this simplifies the imposing of interface boundary conditions. Of course, it would be even more attractive to construct pseudospectral penalty schemes for Helmholtz equations directly. A possible way is first identifying well-posed boundary operators for vectorial second-order wave equations which are the time-domain representation of Helmholtz equations. Once the well-posed operators for the second-order wave equations are identified, a pseudospectral penalty scheme may be formulated for the second-order wave equations. We can then easily convert the time-domain scheme to frequency-domain equations, which becomes a pseudospectral penalty scheme for the equivalent Helmholtz equations. We are putting our effort on this subject and hope to report the results in the future.

VI. Conclusion

A multidomain PSFD method has been developed based on the Legendre polynomials and a penalty scheme for solving Maxwell's equations. The application is particularly aimed at electromagnetic wave scattering problems in plasmonics with the goal of obtaining high-accuracy near fields. Calculation of light scattering by a silver circular cylinder has demonstrated that this PSFD method indeed provides high-order accuracy with the obtained field error down to 10^{-9} referring to 1-V/m incident electric field strength, thanks to the spectral convergence property of the spectral method and the accurate fulfillment of the field continuity conditions across the material interfaces provided by the multidomain approach as well as global

interpolation by Legendre polynomials. In the multidomain approach, the whole computational domain is properly partitioned into curvilinear subdomains fitting the generally curved material-interface shapes. With this demonstrated extremely high numerical accuracy, the formulated method should be useful for plasmonics research and can provide reliable results for the calculation of field enhancement near metal surface, as shown in the numerical examples including coupled plasmonic cylinders of either circular or square shape. Our analysis results also provide a good reference for other numerical methods to compare with. Moreover, the frequency-domain approach has the advantage of directly using a given complex dielectric constant of the material in the calculation with no need of implementing a dispersive material model like in the time-domain approach.

A final remark goes to the possible singular-field behavior when the material interface is non-smooth such as in the square-shaped-cylinder cases, as was discussed in connection with Fig. 5. Although the spectral convergence property of the PSFD method has been demonstrated when simulating round cylinders, when interface corners appear, numerical convergence would unavoidably be degraded. In Fig. 5(c), it was demonstrated that, although only one subdomain is employed for the square-cylinder cross-section, the singular-field characteristic evolves as the degree N in the PSFD calculation is increased so that the grid size near the dielectric corner shrinks. Related treatment of such singularities based on the finite element method has been reported through using algebraically graded grids near the corner where a singularity exists [38]–[40]. Further treatment and more detailed study about the corner singularities using the PSFD method, such as with refined arrangement of subdomains, would worth being pursued as a more basic topic.

ACKNOWLEDGMENT

The authors would like to thank the National Center for High-Performance Computing, Hsinchu, Taiwan, the Academia Sinica Computing Center, Taipei, Taiwan, and the Computer and Information Networking Center, National Taiwan University, Taipei, for providing useful computing resources.

REFERENCES

[1] S. A. Maier and H. A. Atwater, "Plasmonics: Localization and guiding of electromagnetic energy in metal/dielectric structures," *J. Appl. Phys.*, vol. 98, no. 1, Jul. 2005, Art. ID 011101.

[2] M. Moskovits, "Surface-enhanced spectroscopy," *Rev. Mod. Phys.*, vol. 57, no. 3, pp. 783–826, July 1985.

[3] P. Mühlschlegel, H. J. Eisler, O. J. F. Martin, B. Hecht, and D. W. Pohl, "Resonant optical antennas," *Science*, vol. 308, pp. 1607–1609, 2005.

[4] S. A. Maier, P. G. Kik, and H. A. Atwater, "Optical pulse propagation in metal nanoparticle chain waveguides," *Phys. Rev. B*, vol. 67, p. 205402, 2003.

[5] J. P. Kottmann and O. J. F. Martin, "Retardation-induced plasmon resonances in coupled nanoparticles," *Opt. Lett.*, vol. 26, no. 14, pp. 1096–1098, July 2001.

[6] C. F. Bohren and D. R. Huffman, *Absorption and Scattering of Light by Small Particles*. New York: Wiley, 1983.

[7] R. L. Chern, X. X. Liu, and C. C. Chang, "Particle plasmons of metal nanospheres: Application of multiple scattering approach," *Phys. Rev. E*, vol. 76, 2007, Art. ID 016609.

[8] R. Gomez-Medina, M. Laroche, and J. J. Saenz, "Extraordinary optical reflection from sub-wavelength cylinder arrays," *Opt. Exp.*, vol. 14, no. 9, pp. 3730–3737, May 2006.

[9] A. Taflove and S. C. Hagness, *Computational Electrodynamics: The Finite-Difference Time-Domain Method*, 3rd ed. Norwood, MA: Artech House, 2005.

[10] M. Y. Ng and W. C. Liu, "Local-field confinement in three-pair arrays of metallic nanocylinders," *Opt. Exp.*, vol. 14, no. 10, pp. 4504–4513, May 2006.

[11] J. P. Kottmann and O. J. F. Martin, "Plasmon resonant coupling in metallic nanowires," *Opt. Exp.*, vol. 8, no. 12, pp. 655–663, Jun. 2001.

[12] M. W. Chen, Y. F. Chau, and D. P. Tsai, "Three-dimensional analysis of scattering field interactions and surface plasmon resonance in coupled silver nanospheres," *Plasmonics*, vol. 3, pp. 157–164, Oct. 2008.

[13] R. Rodriguez-Oliveros and J. A. Sanchez-Gil, "Localized surface-plasmon resonances on single and coupled nanoparticles through surface integral equations for flexible surfaces," *Opt. Exp.*, vol. 19, no. 13, pp. 12208–12219, Jun. 2011.

[14] J. P. Kottmann, O. J. F. Martin, D. R. Smith, and S. Schultz, "Plasmon resonances of silver nanowires with a nonregular cross section," *Phys. Rev. B*, vol. 64, 2001, Art. ID 235402.

[15] E. Prodan, C. Radloff, N. J. Halas, and P. Nordlander, "A hybridization model for the plasmon response of complex nanostructures," *Science*, vol. 302, no. 5644, pp. 419–422, Oct. 2003.

[16] B. Yang, D. Gottlieb, and J. S. Hesthaven, "Spectral simulations of electromagnetic wave scattering," *J. Comput. Phys.*, vol. 134, pp. 216–230, 1997.

[17] B. Yang and J. S. Hesthaven, "A pseudospectral method for time-domain computation of electromagnetic scattering by bodies of revolution," *IEEE Trans. Antennas Propagat.*, vol. 47, no. 1, pp. 132–141, Jan. 1999.

[18] J. S. Hesthaven, P. G. Dinesen, and J. P. Lynov, "Spectral collocation time-domain modeling of diffractive optical elements," *J. Comput. Phys.*, vol. 155, pp. 287–306, Nov. 1999.

[19] G. Zhao and Q. H. Liu, "The 3-D multidomain pseudospectral time-domain algorithm for inhomogeneous conductive media," *IEEE Trans. Antennas Propagat.*, vol. 52, no. 3, pp. 742–749, Mar. 2004.

[20] Q. H. Liu, "A pseudospectral frequency-domain (PSFD) method for computational electromagnetics," *IEEE Antennas Wireless Propagat. Lett.*, vol. 1, pp. 131–134, 2002.

[21] P. J. Chiang, C. P. Yu, and H. C. Chang, "Analysis of two-dimensional photonic crystals using a multidomain pseudospectral method," *Phys. Rev. E*, vol. 75, Feb. 2007, Art. ID 026703.

[22] P. J. Chiang, C. L. Wu, C. H. Teng, C. S. Yang, and H. C. Chang, "Full-vectorial optical waveguide mode solvers using multidomain pseudospectral frequency-domain (PSFD) formulations," *IEEE J. Quantum Electron.*, vol. 44, no. 1, pp. 56–66, Jan. 2008.

[23] C. H. Teng, B. Y. Lin, H. C. Chang, H. C. Hsu, C. N. Lin, and K. A. Feng, "A Legendre pseudospectral penalty scheme for solving time-domain Maxwell's equations," *J. Sci. Comput.*, vol. 36, pp. 351–390, 2008.

[24] J. P. Berenger, "A perfectly matched layer for the absorption of electromagnetic waves," *J. Comput. Phys.*, vol. 114, no. 2, pp. 185–200, Oct. 1994.

[25] S. Abarbanel and D. Gottlieb, "A mathematical analysis of the PML method," *J. Comput. Phys.*, vol. 134, pp. 357–363, 1997.

[26] S. Abarbanel and D. Gottlieb, "On the construction and analysis of absorbing layers in CEM," *Appl. Numer. Math.*, vol. 27, pp. 331–340, 1998.

[27] L. Rayleigh, "The dispersal of light by a dielectric cylinder," *Philos. Mag.*, vol. 36, pp. 365–376, 1918.

[28] J. R. Wait, "Scattering of plane wave from a circular dielectric cylinder at oblique incidence," *Can. J. Phys.*, vol. 33, no. 5, pp. 189–195, 1955.

[29] W. J. Gordon and C. A. Hall, "Transfinite element methods: Blending function interpolation over arbitrary curved element domains," *Numer. Math.*, vol. 21, pp. 109–129, 1973.

[30] S. Dey and R. Mittra, "A locally conformal finite-difference time-domain (FDTD) algorithm for modeling three-dimensional perfectly conducting objects," *IEEE Microw. Guided Wave Lett.*, vol. 7, pp. 273–275, Sept. 1997.

[31] Y. Liu, C. D. Sarris, and G. V. Eleftheriades, "Triangular-mesh-based FDTD analysis of two-dimensional plasmonic structures supporting backward waves at optical frequencies," *J. Lightw. Technol.*, vol. 25, no. 3, pp. 938–946, Mar. 2007.

[32] Y. Zhao and Y. Hao, "Finite-difference time-domain study of guided modes in nano-plasmonic waveguides," *IEEE Trans. Antennas Propagat.*, vol. 55, no. 11, pp. 3070–3077, Nov. 2007.

[33] W. J. Gordon and C. A. Hall, "Transfinite element methods: Blending-function interpolation over arbitrary curved element domains," *Numer. Math.*, vol. 21, pp. 109–129, 1973.

[34] P. B. Johnson and R. W. Christy, "Optical constants of the noble metals," *Phys. Rev. B*, vol. 6, no. 12, pp. 4370–4379, Dec. 15, 1972.
[35] E. D. Palik, *Handbook of Optical Constants of Solids*. New York: Academic, 1985.
[36] N. N. Rao, *Elements of Engineering Electromagnetics*, 6th ed. Upper Saddle River, NJ: Prentice-Hall, 2004.
[37] J. B. Andersen and V. V. Solodukhov, "Field behavior near a dielectric wedge," *IEEE Trans. Antennas Propagat.*, vol. 26, no. 4, pp. 598–602, Jul. 1978.
[38] W. S. Don and A. Solomonoff, "Accuracy and speed in computing the Chebyshev collocation derivative," *SIAM J. Sci. Comput.*, vol. 16, no. 6, pp. 1253–1268, 1995.
[39] J. S. Hesthaven, "A stable penalty method for the compressible Navier-Stokes equations: III. Multidimensional domain decomposition schemes," *SIAM J. Sci. Comput.*, vol. 20, no. 1, pp. 62–93, 1998.
[40] J. S. Hesthaven and T. Warburton, "Nodal high-order methods on unstructured grids: I. Time-domain solution of Maxwell's equations," *J. Comput. Phys.*, vol. 181, pp. 186–221, 2002.
[41] D. Funaro and D. Gottlieb, "A new method of imposing boundary-conditions in pseudospectral approximations of hyperbolic-equations," *Math. Computation*, vol. 51, pp. 599–613, 1988.
[42] J. S. Hesthaven, S. Gottlieb, and D. Gottlieb, *Spectral Methods for Time-Dependent Problems*. Cambridge, U.K.: Cambridge Univ., 2007.
[43] D. Gottlieb, M. Gunzburger, and E. Turkel, "On numerical boundary treatment of hyperbolic systems for finite difference and finite element methods," *SIAM J. Numer. Anal.*, vol. 19, no. 4, pp. 671–681, 1982.
[44] T. Apel and S. Nicaise, "The finite element method with anisotropic mesh grading for elliptic problems in domains with corners and edges," *Math. Methods Appl. Sci.*, vol. 21, pp. 519–549, 1998.
[45] T. Apel, A.-M. Sandig, and J. R. Whiteman, "Graded mesh refinement and error estimates for finite element solutions of elliptic boundary value problems in non-smooth domains," *Math. Methods Appl. Sci.*, vol. 19, pp. 63–85, 1996.
[46] K. Schmidt and P. Kauf, "Computation of the band structure of two-dimensional photonic crystals with HP finite elements," *Comput. Methods Appl. Mech. Eng.*, vol. 198, pp. 1249–1259, 2009.

Chih-Yu Wang received the B.S. degree from the Department of Engineering Science, National Cheng Kung University, Taiwan, in 2004, and the M.S. and Ph.D. degrees from the Graduate Institute of Electronics Engineering, National Taiwan University, Taiwan, in 2006 and 2012, respectively.

Her current research interests include the pseudospectral electromagnetics modeling in frequency domain.

Shih-Yung Chung received the B.S. degree from the Department of Electrical Engineering, National Cheng Kung University, Tainan, Taiwan, in 2004, and the M.S. and Ph.D. degrees from the Graduate Institute of Electronics Engineering, National Taiwan University, Taipei, Taiwan, in 2006 and 2012, respectively.

His current research interests include the electromagnetic simulations using the pseudospectral time-domain method.

Chun-Hao Teng was born in Tainan, Taiwan, on February 14, 1970. He received the diploma in mechanical engineering from National Taipei Institute of Technology, Taipei, Taiwan, in 1990, the M.S. degree in mechanical engineering from Clarkson University, Potsdam, NY, in 1996, and the M.S. and Ph.D. degrees in applied mathematics from Brown University, Providence, RI, in 2001.

From 2003 to 2009, he was an Assistant Professor with the Department of Mathematics, National Cheng Kung University, Tainan, Taiwan. He is currently an Assistant Research Fellow with the Center of Mathematical Modeling and Scientific Computing, National Chiao Tung University, Hsinchu, Taiwan. His research interests are the developments and applications of high-order numerical methods for partial differential equations.

Juen-Kai Wang was born in Tainan, Taiwan, on July 9, 1961. He received the B.S. degree in electrical engineering from National Taiwan University, Taipei, Taiwan, in 1983, and the M.S. and Ph.D. degrees in applied physics from Harvard University, Cambridge, MA, in 1986 and 1992, respectively.

From 1992 to 1994, he was with Arthur Amos Noyes Laboratory of Chemical Physics, California Institute of Technology, Pasadena. In December 1994, he joined the faculty of the Center for Condensed Matter Sciences, National Taiwan University, Taipei, Taiwan, where he is currently a Research Fellow. He is also jointly appointed with the Institute of Atomic and Molecular Sciences (IAMS) of Academia Sinica. He has acted as a consultant to Industrial Technology Research Institute since 2002. His current research interests include nanometer-scaled optical spectroscopy, ultrafast laser spectroscopy, surface-enhanced Raman spectroscopy, plasmonics, surface vibrational spectroscopy, biomedical vibrational spectroscopy, physical studies of organic semiconductors and their photovoltaic applications, and intense laser interaction with matters.

Dr. Wang was the recipient of the Executive Yuan Award for Outstanding Contributions in Science and Technology in 2009 and the Nano-Tech Award in 2010 that he shared with Dr. Yuh-Lin Wang of IAMS and Prof. Chi-Hung Lin of National Yang-Ming University for their contribution in developing high-speed detection technology for microbiology.

Chung-Ping Chen (M'96) received the B.S. degree in computer science and information engineering from National Chiao-Tung University, Hsinchu, Taiwan, in 1990, and the M.S. and Ph.D. degrees in computer science from the University of Texas, Austin, in 1996 and 1998, respectively.

From 1996 to 1999, he was with Strategic Computer-Aided Design (CAD) Labs, Intel Corporation, Hillsboro, OR, as a Senior CAD Engineer. Since 1999, he has been an Assistant Professor with the Department of Electrical and Computer Engineering, University of Wisconsin, Madison. Since 2003, he has been an Associate Professor with the Electrical Engineering Department, National Taiwan University, Taipei, Taiwan. Currently, he is a Professor with the Graduate Institute of Electronics Engineering, Biomedical Electronics and Bioinformatics and Electrical Engineering Departments, National Taiwan University. His research interests include the areas of electronic design automation and BIO topics, including computer-aided design and microprocessor circuit design with an emphasis on interconnect and circuit optimization, circuit simulation, statistical design, and signal/power/thermal integrity analysis and optimization.

Dr. Chen was the recipient of the D2000 Award from Intel Corporation and the National Sciences Foundation Faculty Early Career Development awards (CAREER) from 1999 to 2001, respectively. He also received the 2002 Special Interest Group on Design Automation/ACM Outstanding Young Faculty Award and the 2002 IBM Peter Schneider Faculty Development Award. He served the program committee and is an organizer of the Design Automation Conference, the International Conference on Computer-Aided Design, Design, Automation, and the Test in Europe Conference, the International Symposium on Physical Design, the Asia and South Pacific Design Automation Conference, the International Symposium on Quality Electronic Design, Synthesis and System Integration of Mixed Information, the VLSI/CAD Symposium, and the International Technology Roadmap for Semiconductors Conference.

Hung-Chun Chang (S'78–M'83–SM'00) was born in Taipei, Taiwan, on February 8, 1954. He received the B.S. degree from National Taiwan University, Taipei, Taiwan, in 1976, and the M.S. and Ph.D. degrees from Stanford University, Stanford, CA, in 1980 and 1983, respectively, all in electrical engineering.

From 1978 to 1984, he was with the Space, Telecommunications, and Radioscience Laboratory of Stanford University. In August 1984, he joined the faculty of the Electrical Engineering Department, National Taiwan University, Taipei, Taiwan, where he is currently a Distinguished Professor. He was the NTU Himax Chair Professor during 2011. He served as Vice-chairman of the EE Department from 1989 to 1991, and Chairman of the newly established Graduate Institute of Electro-Optical Engineering at the same university from 1992 to 1998. His current research interests include the electromagnetic theory, design, and application of photonic structures and devices for fiber optics, integrated optics, optoelectronics, nanophotonics, and plasmonics.

Dr. Chang is a Fellow of the Optical Society of America and the Electromagnetics Academy. He served as the IEICE (Japan) Overseas Area Representative in Taipei from 2002 to 2007.